Preface

Cancer detection and treatment have been greatly enhanced by advances in imaging technology during the last decade. *Image-Guided Diagnosis and Treatment of Cancer* aims to describe the past, current, and future applications of imaging in the diagnosis, staging, treatment, and outcome assessment of cancer of the prostate, central nervous system, and breast. Given the multitude of advances in image-guided biopsy and treatment, this book aims to be the first of its kind to introduce the field of minimally invasive image-guided surgery to the medical community.

Earlier detection using screening mammography has decreased breast cancer mortality (Chapter 3). Approaches to breast cancer detection using magnetic resonance imaging (MRI) are currently under study (Chapter 4). Improved visualization of the prostate gland first using transrectal ultrasound (Chapters 1 and 6) and later using MRI (Chapters 2 and 7) has provided the ability to diagnose prostate cancer and perform minimally invasive delivery of high-dose radiation to the tumor bearing region(s) of the prostate with minimal toxicity. MRI-guided resection of neoplasms and sites of functional disorders allows for minimally invasive biopsy (Chapter 5) and neurosurgery (Chapters 8 and 9) with maximum benefits.

As imaging technology has become increasingly sophisticated, the ability to assess response to chemotherapy (Chapter 10), map temperature profiles (Chapter 11), and visualize gene expression in vivo is becoming a reality (Chapter 12). *Image-Guided Diagnosis and Treatment of Cancer* outlines the current clinical applications of image guidance in the detection (Part I) and treatment (Part II) of carcinoma of the prostate, central nervous system, and breast in order to define the future paradigm of genetic-based imaging and its potential clinical applications (Part III).

Anthony V. D'Amico, *MD, PhD*

Jay S. Loeffler, *MD*

Jay R. Harris, *MD*

2

Magnetic Resonance-Guided Prostate Biopsy

Clare M. Tempany, MD, and Steven Haker, PhD

INTRODUCTION

The goal of a cancer detection program is to detect and diagnose cancer at an early, treatable stage. Prostate cancer is routinely diagnosed by needle biopsy after the detection of either an abnormal prostate-specific antigen (PSA) level or a palpable nodule in the gland. The current standard method to obtain the tissue diagnosis is to sample the prostate gland using transrectal ultrasound (TRUS) imaging guidance. Although this method is the standard clinical approach, this chapter will describe a novel diagnostic method using magnetic resonance imaging guidance that is currently being evaluated in a prospective National Cancer Institute clinical trial.

Prostate Cancer Diagnosis and Treatment

Prostate cancer is the most common noncutaneous malignancy diagnosed in American men. It is estimated that approx 189,000 men were diagnosed in 2002 with prostate cancer *(1)*, although it is also estimated that this figure may be low because of inadequate methods of detection. Currently, either TRUS-guided biopsy or sampling during transurethral prostatectomy are the two most common methods used to diagnose prostate cancer. In the presence of high PSA levels, current biopsy methods are significantly limited by a false-negative rate estimated to be as high as 15 to 31%. TRUS biopsies are specifically limited by low sensitivity of 60%, with only 25% positive predictive value. Studies have shown, moreover, that in more than 20% of cases in which cancer was suspected, at least two biopsy sessions were required to diagnose the tumor *(2,3)*. The TRUS approach does not target focal lesions in the gland; rather, it samples the gland in a sextant manner: bilaterally at the base, the midgland, and the apex. A randomized study of the efficacy of six vs twelve cores in 160 patients showed no difference in cancer detection, thus suggesting that it is the location or target that is actually biopsied, rather than the actual number of samples that matters *(4)*.

Clearly, the difficulty in reaching a definitive diagnosis is not resolved by simply increasing the number of samples taken.

Many men are faced with a dilemma after they have had a negative transrectal prostate biopsy prompted by an abnormal PSA level. Should the patient and his physician

From: *Image-Guided Diagnosis and Treatment of Cancer*
Edited by: A. D'Amico, J. S. Loeffler, and J. R. Harris © Humana Press Inc., Totowa, NJ

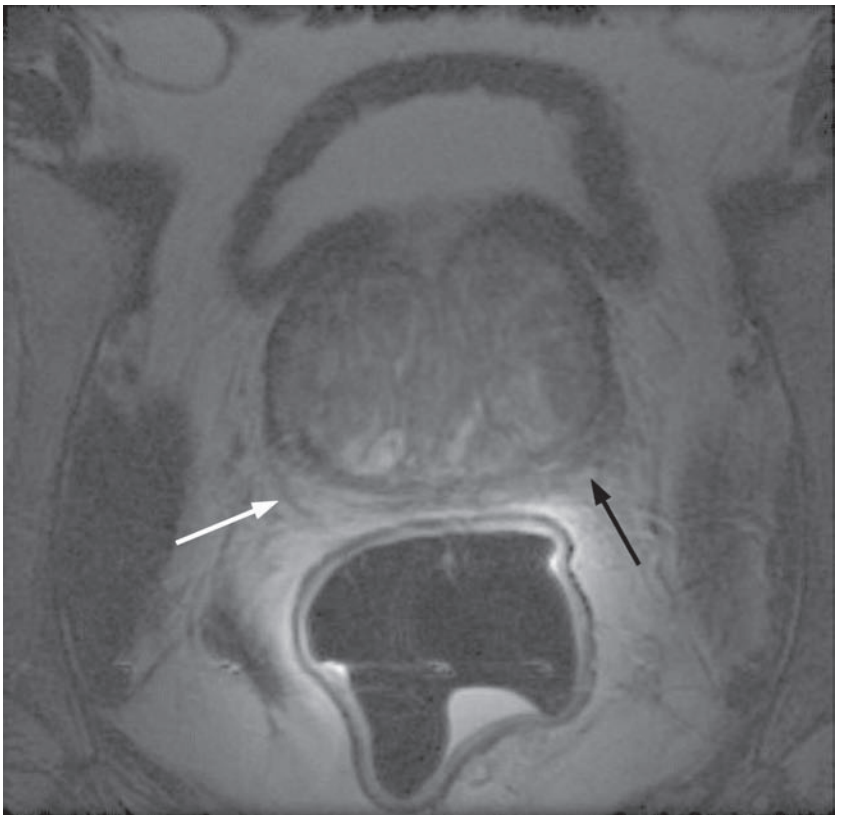

Fig. 1. Axial T2W image with an endorectal coil at 1.5 T. Lower signal intensity in the left PZ (black arrow) compared with right (white arrow) indicates a tumor.

have confidence in the results of the original biopsy in the presence of abnormal PSA levels? In the context of this question, we present a novel biopsy method in such a way that abnormal tissue is depicted in advance of the actual procedure. Then using this information, a targeted and sampling biopsy can be performed. We hypothesis that by using magnetic resonance imaging (MRI), the more precise target definition will improve both the speed and accuracy with which a diagnosis is reached. More timely diagnosis and treatment, in turn, should be to the benefit of the patient in terms of prognosis and quality of life.

MRI OF THE PROSTATE

Significant advances have been made in MRI of the prostate gland in the past decade. It is now clearly established that a combination of T1- and T2-weighted (T1W and T2W) images in multiple planes provide a comprehensive set of images of the entire prostate and its substructure, including the central gland and the peripheral zone. MRI can provide full visualization of the rectum, bladder, seminal vesicles, and neurovascular bundles *(5,6)*. The technology behind MRI has improved significantly, with current state-of-the-art images acquired with an endorectal coil/phased array coil combination

Fig. 2. Axial T2W image with an endorectal coil at 1.5 T showing normal prostate substructure. Specifically, high-signal intensity PZ (black arrows) typical CG heterogeneous signal BPH (white arrows).

at 1.5 T. The combination of the endorectal and multicoil array has been shown to provide the most accurate imaging technique for visualizing and staging the patient's tumor *(7)*. The T2W images allow clear visualization of the peripheral zone (PZ) of the prostate, where over 75% of cancers arise. MRI can detect suspicious lesions in the PZ of the gland on T2W images. Focal (low-signal) lesions in the PZ are suspicious for tumor, especially when located posteriorly in the gland. The sensitivity of MRI for the detection of cancer is relatively high, but the specificity for diagnosis of cancer is not as high. We and others have previously shown that the detection of tumor foci on MRI is, in part, a function of size, with 89% of foci greater than 10 mm and 62% of foci less than 5 mm being detected *(8,9)*. Because PZ is the most common site of origin of prostate cancer among the three prostate zones (PZ, central zone [CZ], and transitional zone [TZ]), localizing and targeting PZ and tumor foci in prostate biopsy may increase the cancer detection rate. For these reasons and those related to the problems of TRUS, we, and others have sought alternative biopsy approaches. We can now perform MR-guided biopsies in an open, interventional MRI unit, which allows for MR-guided needle placement and sampling of biopsy sites *(10–13)* (Figs. 1–6).

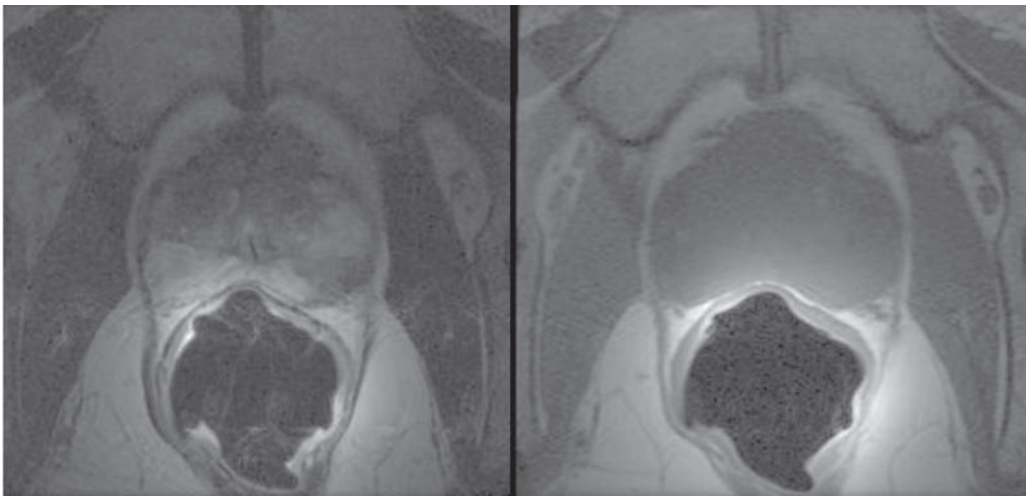

Fig. 3. Axial images with endorectal coil at 1.5 T. On the left, a T2W image, on the right, a T1W image. The same craniocaudial postion is presented.

CURRENT TECHNIQUES TO IMPROVE MR CANCER DETECTION

In an effort to provided greater tumor detection and characterization, there are several new noninvasive imaging techniques currently being tested. These include MR spectroscopy, T2 mapping, diffusion imaging, and intravenous contrast enhancement with gadolinium.

PROSTATE MR SPECTROSCOPY

Several groups have shown the utility of 1H spectroscopy to detect biochemical markers in the prostate that can be used to differentiate prostate cancer from normal tissue or from benign prostatic hyperplasia (BPH) in vivo *(14,15)*. The primary metabolite signal from normal tissue and BPH is the citrate resonance at 2.6 ppm. The primary metabolite signal from prostate cancer is the choline resonance at 3.2 ppm. The ratio of the areas under these two resonances has proven to be a statistically significant indicator for the presence or absence of cancer. Other metabolites that can be detected and quantified with 1H spectroscopy include myo-inositol, creatine, and lipid resonances. Quantification of these resonances and the subsequent formation of various metabolite ratios should further enhance the likelihood of localizing regions where prostate cancer will be encountered with MR-guided biopsies.

T2 MAPPING OF THE PROSTATE GLAND

A British group has produced intriguing results that suggest a positive correlation between the concentration of citrate, as determined by 1H spectroscopy, and the water T2 value, as mapped with multi-echo imaging methods. Because citrate is the so-called good metabolite of the prostate gland, presenting the strongest metabolite signal in normal tissue and BPH *(16–19)*, a decrease in the citrate signal provides an indirect indication of potential PC. Thus, if the correlation between citrate concentration and water T2 values can be independently established, we will improve the spatial resolu-

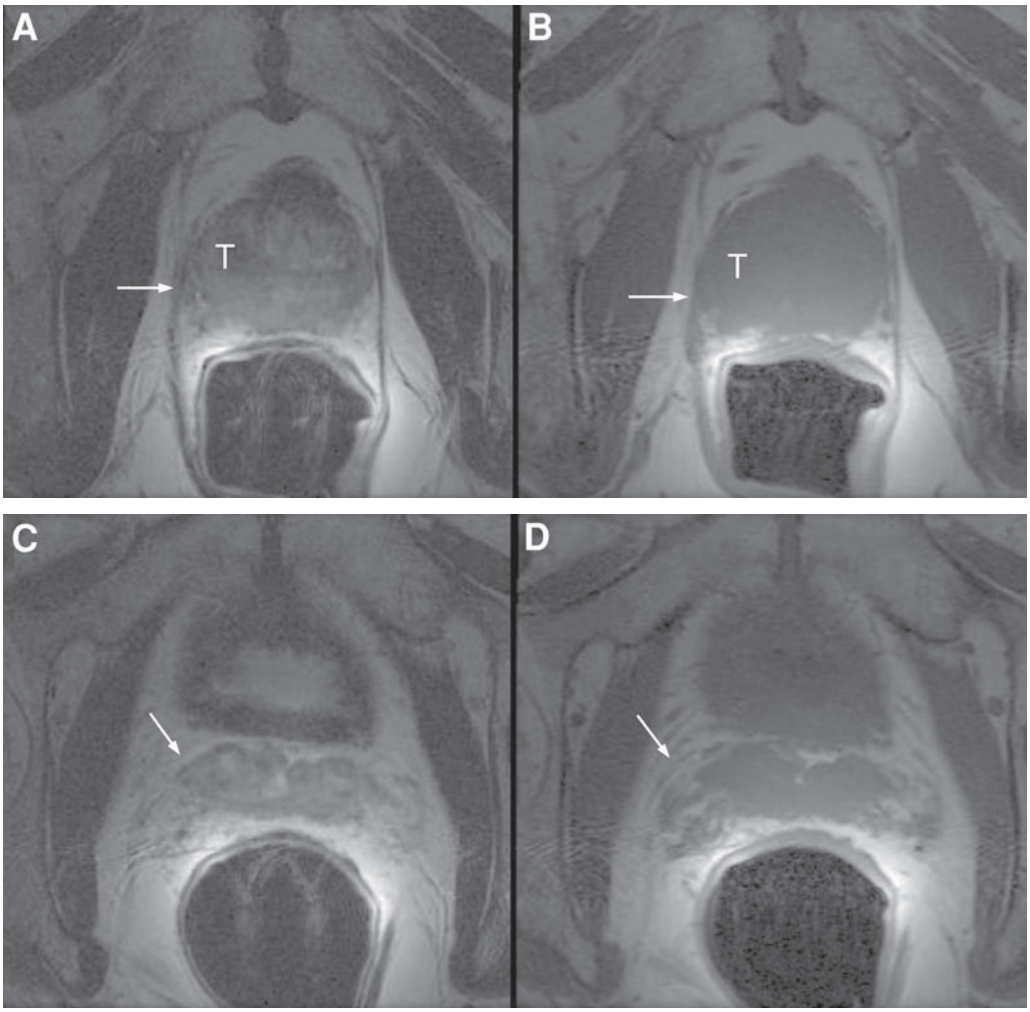

Fig. 4. Axial T2W **(A, C)** T1W **(B, D)** images with an endorectal coil at 1.5 T acquired at the midgland seminal vesicles levels. Images demonstrate a large extensive tumor arising on the right side (T), which invades both the capsule and the seminal vesicles (white arrows).

tion with which suspicious regions of the prostate can be identified for biopsy. Hence, we perform high spatial resolution imaging with fast spin echo sequences at multiple effective echo times to generate quantitative T2 maps of the prostate gland. From these maps, we will identify regions corresponding to spectroscopically interrogated voxels. Currently, we are seeking a correlation between the T2 values of these regions and the metabolite ratios obtained from the two dimensional chemical shift imaging studies, which are currently the best differential indices for prostate cancer vs normal tissue or BPH.

DIFFUSION IMAGING OF THE PROSTATE GLAND

MRI methods for obtaining tissue contrast reflecting water molecular diffusion have become essential for assessing acute stroke in the brain. More recently, evidence has been presented that suggests diffusion imaging may also play a role in the early detec-

Fig. 5. Axial T1W image with pelvic multicoil array, same patient as in Fig. 4. This image shows an enlarged metastatic lymph node in the right external iliac chain (arrow).

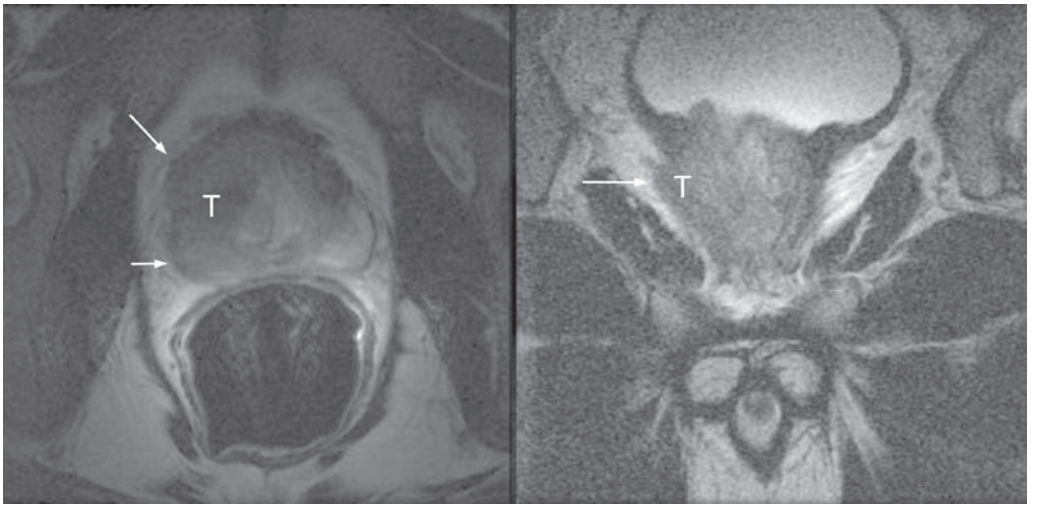

Fig. 6. Axial (left) and coronal (right) T2W images, with an endorectal coil at 1.5 T. Patient is a 56-yr-old man with prostate cancer. This staging MRI shows a large right-sided tumor (T). This tumor involves both the PZ and TZ on the right. Both images show extra-capsular extension of disease (white arrows). Thus, this patient has T3 disease.

tion of brain tumor response to therapy *(20)*. Such successes have encouraged the pursuit of diffusion imaging for characterizing pathology in the prostate. However, technical limitations have largely confined diffusion studies to the brain with only very limited studies of other organs. As a result a technique that overcomes these limitations has been developed and so opens up the possibility of making meaningful water diffusion studies of the prostate possible. To measure tissue water diffusion or the so-called apparent diffusion coefficient (ADC), strong, nonimaging gradient pulses are incorporated that cause a signal reduction related to the overall motion of the water molecules within an imaged pixel. The primary motion of interest for tissue characterization is the microscopic diffusive motion, which is sensitive to the local environment, for example, stroke or tumor environments having different ADCs from that of the surrounding normal tissue. Of course, other artifactual motions may occur during measurement, including respiratory, cardiac, and peristaltic, which will also lead to signal reductions that confound ADC measurements, particularly outside of the brain. Snapshot echo-planar imaging techniques are used to overcome these problems by effectively "freezing" macroscopic motion.

To overcome both the macroscopic motion problem and the inherent limitations of echo-planar imaging diffusion imaging, a new diffusion imaging technique has been developed called line scan diffusion imaging. The technical advantages of line scan diffusion imaging will allow us to make high-quality, high spatial resolution, quantitative diffusion imaging of the prostate *(20)*. This may allow for a meaningful assessment of the prostate tissue ADC parameter as an indicator of cancer and guide for biopsy localization.

Intravenous Contrast Agents

Recent work suggests that by giving intravenous gadolinium T1W images can show different enhancements patterns between cancer and benign tissue. The intravenous contrast is given as a rapid bolus, with multiphase acquisitions, before and after the bolus obtained, using fat suppression. This is preliminary work and may along with the above techniques add further to improve our specificity.

IMAGE-GUIDED PROSTATE INTERVENTIONS

Image-guided therapy has become an important approach for many forms of cancer treatment. The ability to identify the target ahead of time and deliver the maximum therapy to the target is the ultimate goal. The three critical components of any imageguided therapy method are navigation, control, and monitoring of therapy delivery. Precise navigation requires clear identification of the target. To control the delivery of treatment, one needs to accurately identify the target and all adjacent tissues while controlling the intervention or procedure.

Over the past decade, a broad multidisciplinary field of image-guided therapy has evolved from image-guided neurosurgery. At our institution, the image-guided therapy program uses advances in imaging, high-performance computing, and highly evolved new therapy delivery systems to move forward the image-guidance concept into multiple clinical applications *(21,22)*. Image-guided surgery brings powerful technologies into the operating room by taking advantage of advances in computer science and engineering. The simultaneous combination of direct vision and imaging is possible within

a unique environment of intraoperative MRI, which incorporates both the operating room and an imaging system. Open configuration MRI systems are currently in use in several centers in the United States and around the world to guide many types of procedures ranging from diagnostic biopsies of the breast, liver, bone, and other organs to guiding neurosurgical procedures *(11)*. These systems also guide treatment and follow-up treatment effects, in brain and spinal surgery, laser and cryo-ablation of liver tumors and prostate *(23–27)* and breast cancer.

We have developed a computerized software environment for interactive multiplanar three-dimensional (3D) imaging, multimodal visualization, and display. The 3D Slicer is a software program developed in-house by Hata and Gering *(28)*. This system allows for the integration of several facets of image guidance into a single integrated environment. It provides capabilities for automatic registration (aligning data sets), semiautomatic segmentation (extracting structures such as vessels and tumors from the data), generation of 3D surface models (for viewing the segmented structures), and 3D visualization and quantitative analysis (measuring distances, angles, surface areas, and volumes) of various medical scans. The 3D Slicer, now in routine clinical use, has been integrated with the open MRI scanner to augment intraoperative imaging with a full array of preoperative data. The same analysis previously reserved for preoperative data can now be applied to exploring the anatomical changes as the surgery or intervention progresses. The trajectories of the surgical instruments are tracked. By switching the display mode, the real-time scans are visualized in the same 3D view along with the preoperative slices and surface models. The utility of this image-guidance system has been tested for MRI-guided neurosurgery and now under implementation for other image-guided procedures and for several diagnostic applications.

In prostate cancer, it is important to maximize the local treatment effect and to minimize the undesired effects on the normal structures close to the target, thus reducing complication rate. This is the fundamental principle underlying most modern radiation treatment programs for prostate cancer. In 1997, we introduced an MR-guided brachytherapy program for the treatment of localized prostate cancer. We use the MRI in place of ultrasound imaging to delineate the prostate gland and most importantly use the MRI in near-real time to monitor the treatment delivery and radiation dosimetry *(23–27)*.

The ability to use MR to guide biopsies of prostate lesions only detected on MRI is a powerful and useful application of this imaging technology. We are currently using this approach, along with others, in routine clinical practice. A recent pilot study of 33 patients by Perrotti et al. *(10)* showed that MRI could accurately localize tumor foci, with an accuracy of 67%, in patients with previous negative biopsy and elevated serum PSA. They used MRI to identify lesions/targets (based only on signal and not size) and then performed TRUS-guided biopsies attempting to directly biopsy the most suspicious MRI-identified lesions. Prospective evaluation of endorectal MRI to detect tumor foci in men with prior negative prostatic biopsy is described in a pilot study.

MRI-GUIDED BIOPSY

The experience we gained from the MR-guided brachytherapy program led us to believe that by adapting this approach we could perform MR-guided percutaneous prostate biopsies. The brachytherapy procedure demonstrated that it is feasible to place needles into specific targets in the prostate under intraoperative MRI guidance. Among

Table 1
MR-Guided Prostate Biopsy Patient Population

Eligibility criteria
• Either an abnormal serum PSA level (>4 ng/mL) or a palpable nodule in the prostate on digital rectal examination.
• Either previous negative biopsy or no transrectal access for biopsy sampling.
• MRI of the prostate gland, with or without a focal lesion.
• Age >30 yr.
• Informed consent.
• No contraindication to MR-induced anesthesia, that is, no risk of silent ischemia.
Exclusion criteria
• Inability to give informed consent.
• Contraindications to MRI cardiac pacemaker, inner ear implants, non-MR-com patible intracranial aneurysm clips.
• Contraindications to MR-induced anesthesia-epidural or general anesthesia.

the goals of our work is to answer the question of whether improved detection of clinically significant prostate cancers can occur if the biopsy is guided by MRI. As our brachytherapy program developed, it became apparent that this approach had the potential to allow MR-guided prostate biopsies. Thus, in response to a clinical demand, we adapted our system to perform MR-guided biopsies. We anticipate that biopsies based on MRI localization and needle guidance compared with random sextant sampling will be more effective in detecting localized prostate cancer.

BIOPSY PATIENT POPULATION

Our patients are all men with abnormal PSA levels (>4 ng/mL; Hybritech method) from one for the following two groups: 1) Men who have had previous abdominoperineal resection (APR) of the rectum who cannot undergo a TRUS-guided biopsy and 2) Men who have abnormal PSA and have had more than one negative TRUS biopsy. All patients have a prebiopsy MR exam with either the multicoil-phased array alone or a multicoil array and endorectal coil, at 1.5 T. These images provide planning information for the biopsy both for target definition and depiction of the peripheral zone. We exclude from biopsy patients who have any of the standard exclusion criteria for MRI, for example, cardiac pacemakers. We also exclude men with significant cardiac ischemia. All men are evaluated by the anesthesia service, as they do of all men undergoing MR-guided brachytherapy, for the induction of anesthesia in an MR environment. Men with significant cardiac ischemia are excluded because they cannot be adequately monitored in the intraoperative MRI unit.

After patients have the initial MR exam, the biopsy procedure is discussed with them and informed consent is obtained (Table 1).

On the day of the procedure, the patient comes to the intraoperative MRI suite and is prepared for the biopsy. He is positioned in the lithotomy position, with the side entry position of the table. The patient receives either a general or spinal anesthesia, as selected by the anesthesiologist, to keep him from pain and discomfort and to immobilize his pelvis and provide a fixed target that will not move during the procedure. The external MR transmits and receive coil are wrapped around his pelvis, and initial images confirm a good position.

The skin of the perineum is prepared and draped after a Foley catheter has been placed in the bladder. Then a Plexiglas template is fixed up against the patient's perineum. If the rectum is normal, a stiff obturator is placed to allow for clear delineation of the anterior rectal wall and posterior prostate. Then, the prebiopsy images are obtained.

For biopsy localization, each sextant of the prostate gland can be targeted as they are under ultrasound guidance. We image the prostate in the coronal plane and divide the gland into three areas: apex, base, and midgland. We believe we are able to increase the likelihood that the samples are taken from the PZ for the following reasons: we have real-time MRI guidance and we use the 3D Slicer software, which allows for T2W images to be displayed in the operating room. Thus allowing for visualization of the PZ/central gland (CG), as the needle is inserted. As the approach is transperineal, the needles enter the posterior gland and travel in a vertical trajectory through the PZ, increasing the probability that all samples will be taken from the PZ. The real-time imaging with fast gradient recalled (FGR) imaging sequences, the 3D Slicer, and the T2W images are be used to confirm that the samples are being taken from the PZ.

An axial T2W volumetric sequence acquired in the 0.5 T Signa SP Magnetic Resonance Therapy (MRT) System (GE Medical Systems, Milwaukee, WI) at the start of the biopsy procedure is incorporated into the 3D Slicer to provide "virtual" guidance into the PZ of the prostate (Figs. 7 and 8).

As each real-time FGR image is obtained, this T2W sequence is resampled so as to match the spatial position of the FGR image. We alternate the display of the real-time FGR image with the corresponding resampled T2W image to provide the observer with information on the location of the needle, its position within the PZ, and its relation to targets visible on the T2W image. The 18-gage (MR-compatible) biopsy guns are placed into the gland under MR guidance. The real-time imaging sequences are FGRs, which are rapidly acquired and clearly depict the needle; they can be acquired in the axial, sagittal, and coronal planes. The needle artifact is clearly seen on these FGR images. Using the 3D Slicer, we can alternate the image on the in-bore monitor. Thus allowing the radiologist to see both the needle and the prostate substructure simultaneously.

We perform sextant sampling of the gland under MRI guidance in a way similar to TRUS, that is, we target the six locations on the gland. We use 18-gage biopsy guns, the same size used in routine clinical practice, to take the tissue samples. We sample the PZ at the apex, base, and midgland bilaterally. All specimens are labeled, sent to pathology, and handled in the standard clinical fashion (Fig. 9).

INTERVENTIONAL MRI TECHNIQUES

As described earlier, the current state of the art for imaging the prostate requires 1.5-T field-strength MR techniques using a combined endorectal and pelvic array coils. This is routinely performed on all patients in our brachytherapy program. In the development of the MRI-guided brachytherapy program, which uses a 0.5-T filed strength system, we felt that it was important to ensure that the MR sequences and coils would provide adequate images of the prostate. Thus, we compared the image quality in a subset of 20 patients, evaluating each of the studies for ease of identification of the gland, its substructure, and abnormal foci from the endorectal coil 1.5 T images and the 0.5 T images. The total score of conspicuity of normal structures was 27.95 for the 1.5 T images and 26.5 for the 0.5 T images. The mean signal-to-noise ratios (SNRs) for the PZ were 11.1 ± 4.7 at 1.5 T and 10.3 ± 3.8 at 0.5 T ($p = 0.40$). However, the contrast-to-

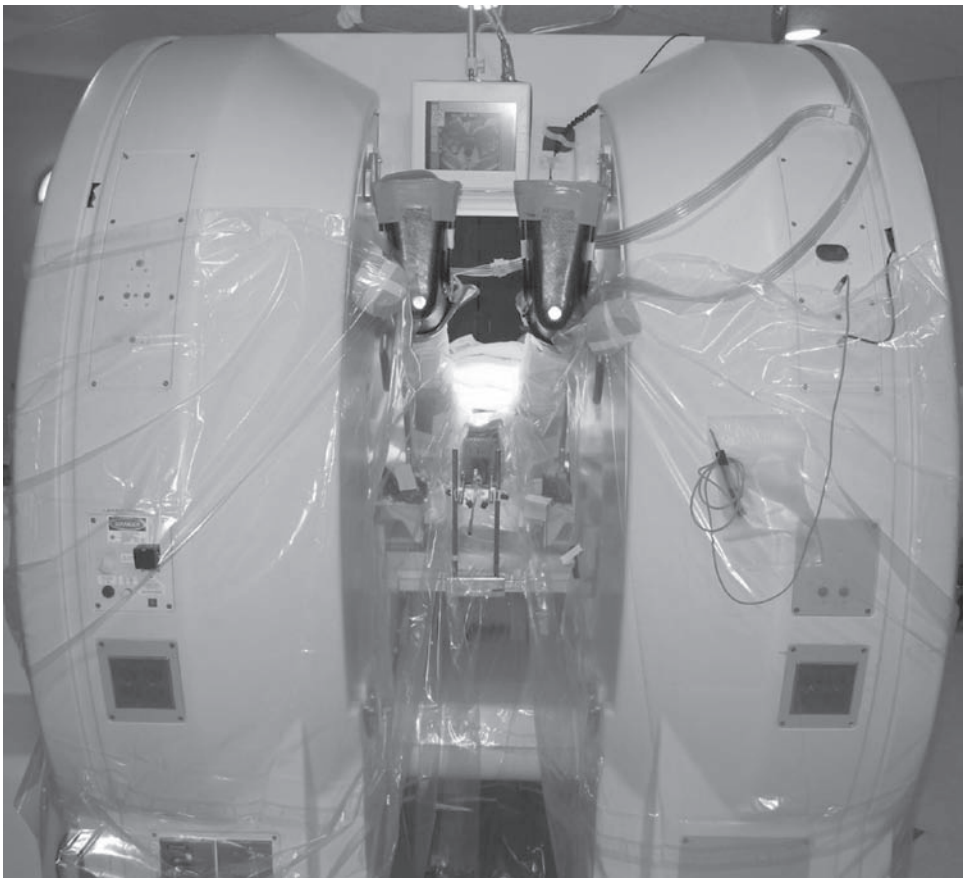

Fig. 7. General Electric Signa SP 0.5 T system with patient in lithotomy position.

noise ratios of the PZ vs the CG were significantly different ($p = 0.002$), being 7.0 ± 4.4 for 1.5T and 4.1 ±- 2.2 at 0.5 T. In almost all aspects the 0.5 T images compared very favorably with the 1.5 T images. The only area where a difference was found was in the identification of focal lesions, in 12 of 20 men suspicious foci were seen at 1.5 T and not at 0.5 T *(27)*. This may be explained in part by the difference in field strength, SNR, and the imaging parameters, which are adapted for the lower field strength and the field of view; the imaging coil used is an external wrap-around coil, not an endorectal coil.

Image Analysis

Multiple biopsy locations are planned from the two image data sets, the 1.5 T data and the 0.5 T data. The latter, obtained on the day of the biopsy, after induction of anesthesia. All the 1.5 T MR images and the 0.5 T images are analyzed by the radiologist for the presence of any focal lesion, defined as any focal area of low T2W signal intensity in the PZ. Any and all lesions are identified, measured, and localized. These are thus the image-based "targets," and at least six sextant locations are also identified, which comprise the list of sites to be sampled.

Also under development is the ability to integrate 1.5 T images into the 0.5 T image display system and into the 3D Slicer visualization program to allow for improved

Fig. 8. Close-up of patient position, with in-bore monitor showing axial image of the prostate.

target definition. Our goals in this area are to achieve automated registration and segmentation for intraoperative treatment planning and to provide preoperative image data in the operating room for navigation to ultimately improve the accuracy and efficiency of the procedure.

3D VISUALIZATION

The real-time imaging sequences are gradient echo sequences, which are excellent for delineating the gland, the rectum, the catheter, and bladder but not the internal zones of the prostate. Therefore, the availability of T2W images provided by the 3D Slicer is critical in targeting the PZ during prostate biopsies.

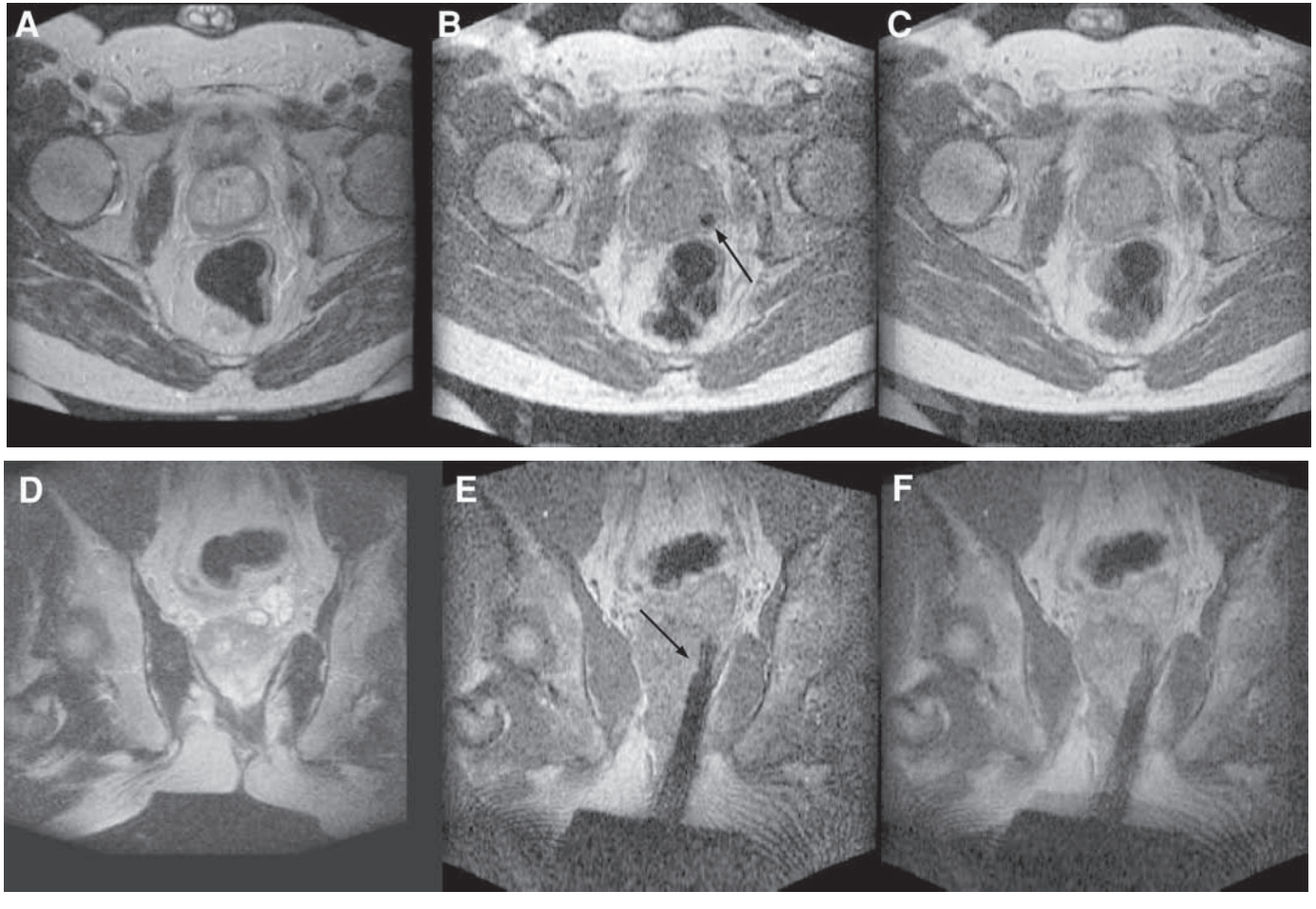

Fig. 9. (**A**) Axial T2W 0.5 T Signa SP image showing high-signal PZ. (**B**) Axial FGR real-time image shows needle artifact (arrow). (**C**) Fused image shows combining axial T2 FGR data. (**D**) Coronal T2W 0.5 T Signa SP image showing high-signal PZ. (**E**) Coronal FGR real-time image shows needle artifact (arrow). **(F**) Fused image shows combining coronal T2 FGR data.

IMAGE INTEGRATION AND FUSION

Image Registration and Segmentation

In performing prostate image segmentation, we are attempting to provide classification of the prostate substructure, which will allow automated definition of the PZ and CG. It will also allow for accurate definition of the prostate boundary and location of adjacent structures.

Segmentation

With the aim of integrating preoperative images into the intraoperative image dataset for navigation, control, and planning, we are working to develop an automated MRI segmentation program to analyze prostate gland, its boundary, and substructure. This approach, which is based on our preliminary investigations, will use the combined data from the pre- and intraprocedural MR images and allow the treatment plan to be based upon the full data set. We follow these steps:

1. Segment the PZ and the CZ/TZ in the 1.5 T preoperative PD/T2W MR images. This segmentation will also yield the outline of the prostate (i.e., the prostate capsule).
2. Deform the segmenting curves in accordance with how the prostate deforms as the patient moves from the supine to the lithotomy position, and
3. Segment the prostate capsule in the 0.5 T intraoperative MR images.
4. Apply rigid registration to match the capsule of the 1.5 T preoperative MR images to the capsule of the 0.5 T intraoperative MR images.

Once the pre- and intraoperative capsule segmentations are aligned, the PZ and the CZ/TZ segmentation of the 1.5 T MR images obtained can be overlaid on top of the 0.5 T MR images to provide the information needed for biopsy, namely, the differentiation of PZ and CZ/TZ in the procedural room.The important structures to be treated, or spared, are segmented by the method described above. These structures include the central and peripheral parts of the prostate, the urethra, and the anterior wall of the rectum. After this segmentation process, the treatment is designed and the dosimetry evaluated and refined as necessary. For rigid registration, a cost functional using similarity measures, such as mutual information, can be designed to capture the essence of a good alignment. By minimizing the cost functional, the two capsules will be aligned. Alternatively we may use an approach based on volume of overlap. Both of these methods have been used extensively in our laboratory in other applications.

Preliminary studies have shown that as the body moves from the supine position to the lithotomy position, the prostate has the tendency to shorten longitudinally, with the upper half of the prostate tilting slightly forward pivoting about the center of the organ. The different zones of the prostate are clearly visible in 1.5 T diagnostic MR images, and the challenge is to integrate this information into the 0.5 T interventional MR images obtained intraprocedurally during biopsy, while the patient is in the lithotomy position. To this end we have investigated methods for segmenting the prostate and simulating its deformation. Our segmentation approach uses a variant of the curve–evolution approach, and incorporates models of the intensity characteristics of the tissues. Previous work in these flows has demonstrated good results in segmenting images that may be differentiated by regions that have different intensity statistics, for example, different vegetations in synthetic aperture radar images *(29–31)*. We have dem-

onstrated the feasibility and performance of these flow algorithms on preoperative prostate MR images. Curves are superimposed on top of each image slice to show the locations of the PZ and CG obtained by applying the algorithm. These contours appear to accurately outline the correct boundaries of the prostate structures. The remaining challenge is to increase the information content of the 0.5 T intraoperative MR images, which have two fundamental problems:

1. In both 1.5 T and 0.5 T MR images, the prostate gland is textured with weak or diffused boundaries that make the segmentation process challenging.
2. It is difficult to capture the nonrigid deformation of the prostate as the patient moves from a supine position to a lithotomy position.

REGISTRATION

The goal is the registration of 1.5 T images into the 0.5 T images, by mapping and deformation of the images. Much of this work is based on our experience with rigid and deformable registration in neurosurgery. Initially, a diagnostic staging MRI is obtained with an endorectal coil, which provides excellent SNR characteristics in the region of the prostate.

Registration techniques are useful when the organ or target of interest moves, changes shape, or has characteristics that vary at different points in time. Our experience in rigid and deformable registration is mostly from neurosurgery. Viola and Wells *(30–32)* have developed a fully automatic rigid registration method for multimodal medical image registration. The method is based on a formulation of the mutual information between the model and the image. The method is intensity based instead of feature based, which has the advantage of not requiring presegmentation of the data. Registration of MR to MR, MR to computed tomography, MR to single-photon emission computed tomography and positron emission tomography, and video to 3D models has be en successfully performed on test data sets and has been used in many cases *(33)*.

In deformable registration, Warfield, Dengler, and Robatino *(34)* implemented Dengler's optical flow-based deformable registration in our high-performance computing setting.

This method constructs and minimizes an energy function in which two terms control goodness-of-matching and elasticity of deformation. The deformation model is a continuous 3D vector field generalization of a controlled continuity functional. Our first major application of the technique was to use nonlinear registration for template driven segmentation. A method to measure spatial and temporal brain deformation from sequential intraoperative MRI has also been developed. Deformation is estimated with a volumetric optical flow measurement based on local intensity differences. The method demonstrated a good capability of intra-operative surface, subsurface and midline shift measurement.

Therefore, a manual and interactive matching tool may be helpful for matching the leg-up and leg-down images. Using this tool, we can start the registration from a better initial guess and thus can expect the more accurate matching in shorter time. Because of the close proximity and the anterior placement of the obturator relative to the prostate, the prostate also displaces posteriorly. In preliminary experiments, this deformation model has been based on physical principles associated with the soft tissue deformation under external force. The external force, in our case, is the obturator. We

model this external force as a point source located in the rectum having a displacement force that falls off at the rate of 1/*r*, with *r* being the distance from the point source. Under the influence of this external force, the soft tissue (i.e., the prostate) deforms. However, as with all soft tissues, the prostate deforms with resistance. The more the prostate deforms, the more it resists the change. Thus many steps have been integrated to allow a detailed and precise registration and segmentation of the prostate imaging data sets.

ACKNOWLEDGMENT

Funding for this research has been provided by NIH grant R01 AG19513.

SUMMARY

As our imaging techniques improve, the role of image guided interventions has increased. We will need tissue sampling for validation and pathological confirmation of disease activity. More importantly, we will need new and noninvasive methods to deliver therapy with image guidance to precise targets.

REFERENCES

1. American Cancer Society website: www.cancer.org. American Cancer Society Inc., Surveillance Research 2002.
2. Terris MK. Sensitivity and specificity of sextant biopsies in the detection of prostate cancer: preliminary report. *Urology* 1999;54:486–489.
3. Keetch DW, McMurtry JM, Smith DS, Andriole GL, Catalona WJ. Prostate specific antigen density versus prostate specific antigen slope as predictors of prostate cancer in men with initially negative prostatic biopsies. *J Urol* 1996;156:428–431.
4. Naughton CK, Smith DS, Humphrey PA, Catalona WJ, and Keetch DW. Clinical and pathologic tumor characteristics of prostate cancer as a function of the number of biopsy cores: a retrospective study. *Urology* 1998;52(5):808–813.
5. Tempany CM, Rahmouni AD, Epstein JI, Walsh PC, Zerhouni EA. Invasion of the neurovascular bundle by prostate cancer: evaluation with MR imaging. *Radiology* 1991;181:107–112.
6. Carter HB, Brem RF, Tempany CM, et al. Nonpalpable prostate cancer: detection with MR imaging. *Radiology* 1991;78:523–525.
7. Hricak H, White S, Vigneron D, et al. Carcinoma of the prostate gland: MR imaging with pelvic phased-array coils versus integrated endorectal–pelvic phased-array coils. *Radiology* 1994;193:703–709.
8. Ellis JH, Tempany C, Sarin MS, Gatsonis C, Rifkin MD, McNeil BJ. MR imaging sonography of early prostatic cancer: pathologic imaging features that influence identification diagnosis. *AJR Am J Roentgenol* 1994;162:865–872.
9. Ikonen S, Karkkainen P, Kivisaari L, et al. Magnetic resonance imaging of clinically localized prostatic cancer. *J Urol* 1998;159:915–919.
10. Perrotti M, Han, K-R, Epstein RE, et al. Prospective evaluation of endorectal magnetic resonance imaging to detect tumor foci in men with prior negative prostastic biopsy: a pilot study. *J Urol* 1999;162:1314–1317.
11. Silverman SG, Collick BD, Figueira MR, et al. Interactive MR-guided biopsy in an open-configuration MR imaging system [see comments]. *Radiology* 1995;197:175–181.
12. D'Amico AV, Cormack RA, Tempany CM. MRI-guided diagnosis treatment of prostate cancer. *N Engl J Med* 2001;344:776–777.

13. Hata N, Jinzaki M, Kacher D, et al. MRI-guided prostate biopsy with surgical navigation software: device validation feasibility. *Radiology* 2001;220:263–268.
14. Kurhanewicz J, Swanson MG, Nelson SJ, Vigneron DB. Combined magnetic resonsnce imaging spectroscopic imaging approach to molecular imaging of prostate cancer. *J Magn Reson Imaging* 2002;16:463.
15. Kaji Y, Kurhanewicz J, Hricak H, et al. Localizing prostate cancer in the presence of postbiopsy changes on MR images: role of proton MR spectroscopic imaging. *Radiology* 1998;206:785–790.
16. Liney GP, Knowles AJ, Manton DJ, Turnbull LW, Blackband SJ, Horsman A. Comparison of conventional single echo multi-echo sequences with a fast spin-echo sequence for quantitative T2-mapping: application to the prostate. *J Magn Reson Imaging* 1996;6: 603–607.
17. Lowry M, Liney GP, Turnbull LW, Manton DJ, Blackband SJ, Horsman A. Quantification of citrate concentration in the prostate by proton magnetic resonance spectroscopy: zonal age related differences. *Magn Reson Med* 1996;36:352–358.
18. Liney GP, Lowry M, Turnbull LW, et al. Proton MR T2 maps correlate with the citrate concentration in the prostate. *NMR Biomed* 1996;9:59–64.
19. Liney GP, Turnbull LW, Lowry M, Turnbull LS, Knowles AJ, Horsman A. In vivo quantitation of citrate concentration water T2 relaxation time of the pathologic prostate gland using ^{1}H MR MRI. *Magn Reson Imaging* 1997;15:1177–1186.
20. Maier SE, Bogner P, Bajzik G, et al. Normal brain brain tumor: multicomponent apparent diffusion coefficient line scan imaging. *Radiology* 2001;219:842–849.
21. Schenck JF, Jolesz FA, Roemer PB, et al. Superconducting open-configuration MR imagingsystem for image-guided therapy. *Radiology* 1995;195:805–814.
22. Jolesz FA. 1996 RSNA Eugene P. Pendergrass New Horizons Lecture. Image-guided procedures the operating room of the future. *Radiology* 1997;204:601–612
23. D'Amico AV, Cormack R, Tempany CM, et al. Real-time magnetic resonance image-guided interstitial brachytherapy in the treatment of select patients with clinically localized prostate cancer. *Int J Radiat Oncol Biol Phys* 1998;42:507–515.
24. Tempany C, D'Amico A, Cormack R, Kumar S, Silverman S, Jolesz F. MR guided prostatebrachytherapy: a new approach to seed implantation. in NE-AUA. 1999;
25. Cormack R, Kooy H, Tempany C, D'Amico A. (1998) A clinical method for real-time dosimetric guidance of transperineal 125I prostate implants using interventional magnetic resonance imaging. *Int J Radiat Oncol Biol Phys* 2000;46(1): 207–214.
26. Hurwitz MD, Cormack R, Tempany CM, Kumar S, D'Amico AV. Three-dimensional real-time magnetic resonance-guided interstitial prostate brachytherapy optimizes radiation dose distribution resulting in a favorable acute side effect profile in patients with clinically localized prostate cancer. *Tech Urol* 2000;6(2):89–94.
27. McTavish J, D'Amico A, Cormack R, Jolesz F, Tempany C. Evaluation of interventional MRI images (0.5T) of the prostate gland compared to endorectal coil MRI images (1.5T) in men undergoing MR guided brachytherapy (abstr), in *Proceedings of the Seventh Meeting of the International Society for Magnetic Resonance in Medicine*, Philadelphia, PA, 1999, p. 1972.
28. Hata N, Wells WM III, Warfield S, Kikinis R, Jolesz FA. Computer assisted intraoperative MR-guidedtherapy: pre- intra-operative image registration, enhanced three-dimensional display, deformable registration, in 7th Annual meeting Japan Society of Computer Aided Surgery. Sapporo, Japan; 1997.
29. Richard WD. Keen CG. Automated texture-based segmentation of ultrasound images of the prostate. *Comput Med Imaging Graph* 1996;20:131–140.
30. Wells WM III, Viola P, Atsumi H, Nakajima S, Kikinis R. Multi-modal volume registration by maximization of mutual information. *Med Image Anal* 1996;1:35–51.

31. Viola P. Wells W. Alignment by maximization of mutual information. *Int J Comp Vision* 1997;24:137–154.
32. Wells WM III, Viola P, Atsumi H, Nakajima S, Kikinis R. Multi-modal volume registration by maximization of mutual information. *Med Image Anal* 1996;1:35–51.
33. Kagawa K Lee WR, Schultheiss TE, Hunt MA, Shaer AH, Hanks GE. Initial clinical assessment of CT–MRI image fusion software in localization of the prostate for 3D conformal radiation therapy. *Int J Radiat Oncol Biol Phys* 1997;38:319–325.
34. Warfield SW, Robatino A, Dengler J, et al. Nonlinear registration and template driven segmentation, in *Brain Warping* (Toga AW, ed.), Academic Press, San Diego, CA, 1999, pp. 67–84.